Femtosecond Laser-Excitation-Driven High Frequency Standing Spin Waves in Nanoscale Dielectric Thin Films of Iron Garnets

Marwan Deb, Elena Popova, Michel Hehn, Niels Keller, S. Petit-Watelot, Matias Bargheer, Stéphane Mangin, Grégory Malinowski

Femtosecond Laser-Excitation-Driven High Frequency Standing Spin Waves in Nanoscale Dielectric Thin Films of Iron Garnets

Marwan Deb,[1,2,*] Elena Popova,[3] Michel Hehn,[1] Niels Keller,[3] Sébastien Petit-Watelot,[1] Matias Bargheer,[2] Stéphane Mangin,[1] and Gregory Malinowski[1]

[1]*Institut Jean Lamour (IJL), CNRS UMR 7198, Université de Lorraine, 54506 Vandœuvre-lès-Nancy, France*

[2]*Institut für Physik und Astronomie, Universität Potsdam, Karl-Liebknecht-Str. 24-25, 14476 Potsdam, Germany*

[3]*Groupe d'Etude de la Matière Condensée (GEMaC), CNRS UMR 8635, Université Paris-Saclay, 78035 Versailles, France*

(Received 16 April 2019; published 10 July 2019)

We demonstrate that femtosecond laser pulses allow triggering high-frequency standing spin-wave modes in nanoscale thin films of a bismuth-substituted yttrium iron garnet. By varying the strength of the external magnetic field, we prove that two distinct branches of the dispersion relation are excited for all the modes. This is reflected in particular at a very weak magnetic field (∼33 mT) by a spin dynamics with a frequency up to 15 GHz, which is 15 times higher than the one associated with the ferromagnetic resonance mode. We argue that this phenomenon is triggered by ultrafast changes of the magnetic anisotropy via laser excitation of incoherent and coherent phonons. These findings open exciting prospects for ultrafast photo magnonics.

DOI: 10.1103/PhysRevLett.123.027202

The continuous demand for more energy efficient and faster data transport and processing devices has triggered intense research activity to carry information with other means than the electron charge, which is associated with an inevitable Joule heating in current semiconductor-based information technologies [1]. One of the most promising ways to achieve this goal is the use of the coherent collective excitation of spins in magnetic materials, commonly known as magnons or spin waves (SWs) [2–5]. These waves can propagate in both metallic and dielectric magnetic media without involving any charge transport, which avoids the Joule heating, and therefore reduces substantially the power consumption for data processing. Besides this energy efficiency, using SWs offers other important advantages for ultrafast nanoscale computation due to their broad high frequency range from GHz to THz and tunable wavelength down to the nanoscale [6]. From a fundamental point of view, SWs exhibit remarkably rich physics involving both dipolar and exchange interactions [6,7]. This is reflected by versatile dispersion relations containing magnetostatic and exchange modes, which can either be tuned by an external magnetic field (H_{ext}) and/or the sample size [3,6]. In this context, intense research is being carried out to understand the generation, propagation, manipulation, and detection of SWs in a continuously growing field of modern magnetism called magnonics [2–5].

Because of its low magnetic damping constant, the yttrium iron garnet (YIG) has attracted a lot of attention in the field of magnonics [8]. Indeed, many important magnetostatic SWs based devices have been realized using YIG during the last decade [9–12]. However, due to the small saturation magnetization of YIG together with the restrictions imposed by the size of the microwave antennas on the excited SWs wavelength with the standard method of microwave magnetic fields, magnetostatic SWs frequencies in such devices did not exceed a few GHz at low field, which is a major limiting factor for ultrafast applications. On the other hand, due to the strong exchange interaction between spins, the exchange SWs mode can have higher frequencies compared to the magnetostatic one. The possibility of triggering such exchange modes requires a nonuniform dynamical field across the magnetic film thickness [13], which is very challenging to induce using microwave antennas [13–15]. Recently, femtosecond laser pulses have been used as an efficient stimulus to excite a coherent spin precession [16,17]. In particular, it was demonstrated that femtosecond laser pulses can excite exchange standing SWs (SSWs) in metallic [18,19] and semiconductor [20,21] ferromagnets via thermal processes. On the other hand, most studies on iron garnets have been dedicated to the excitation and control of the homogenous resonance mode ($k = 0$, i.e., low frequency) via nonthermal excitation mechanisms [22–29]. An important question in this context concerns the possibility to take advantage of femtosecond laser pulses for triggering a high frequency SSW in dielectric thin films of iron garnets.

In this Letter, we demonstrate femtosecond laser-excited high frequency even and odd SSWs in nanoscale films of Bi-substituted yttrium iron garnet (Bi-YIG). Bi-YIG materials have, in addition to a low damping [30], very large magneto-optical Faraday effects [31], which make them well adapted for new photo magnonics devices. By varying the strength of the external applied magnetic field H_{ext}, we demonstrate two distinct branches of the dispersion relation

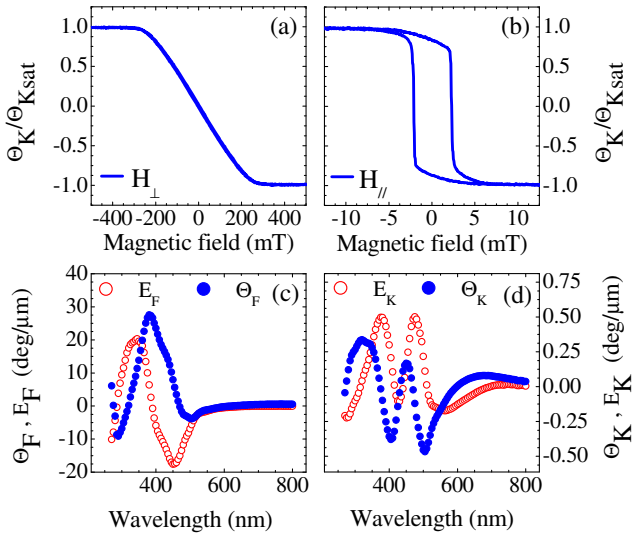

FIG. 1. Static magnetic and magneto-optical properties of the garnet sample. (a),(b) Normalized Kerr hysteresis loop measured in polar (a) and longitudinal (b) configuration. (c),(d) Magneto-optical Faraday (c) and Kerr (d) polar spectra measured over a broad range of wavelength. The filled and open symbols represent, respectively, the ellipticity (E_F, E_K) and rotation (Θ_F, Θ_K).

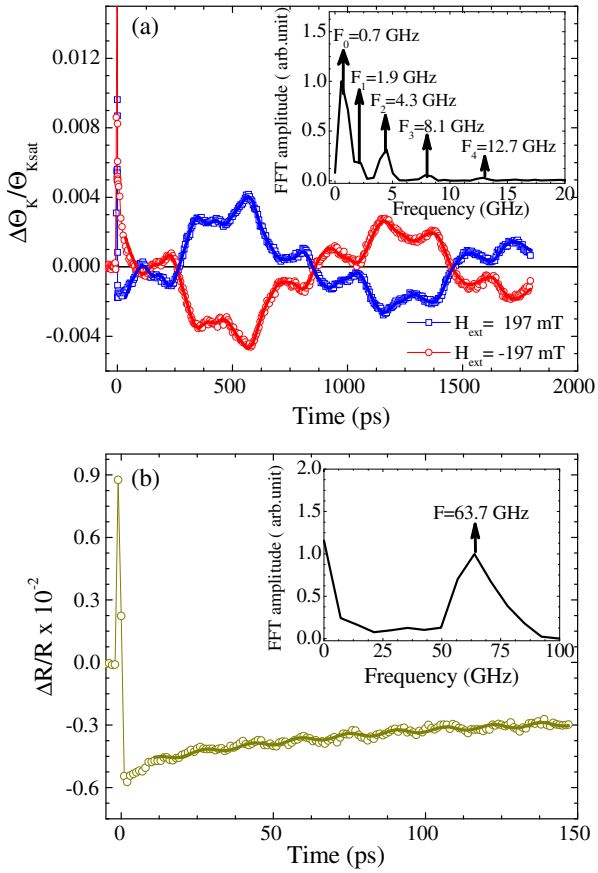

FIG. 2. Laser-induced spin and reflectivity dynamics in the garnet sample. (a),(b) $\Delta\Theta_K/\Theta_{K\mathrm{sat}}$ and $\Delta R/R$ induced by $E_{\mathrm{pump}} = 9.9\ \mathrm{mJ\,cm^{-2}}$ for $H_{\mathrm{ext}} = \pm 197$ mT. The solid lines are fits to the data using Eq. (1) in (a) and Eq. (2) in (b). The insets show the FFT spectra.

for all the SSW modes. We report at very low H_{ext} a spin precession with a frequency of 15 GHz, which is 15 times higher than the one associated with the ferromagnetic resonance (FMR) mode. We demonstrate that this phenomenon is driven by ultrafast changes of magnetic anisotropy via laser excitation of incoherent and coherent phonons.

The Bi-YIG sample studied in our work is a 135-nm thick $Bi_1Y_2Fe_5O_{12}$ single crystalline film, grown by pulsed laser deposition on (100) gadolinium gallium garnet (GGG) substrate (See Supplemental Material [32], Note 1). All the experiments discussed here are performed at room temperature. Figures 1(a) and 1(b) show the normalized polar and longitudinal Kerr hysteresis loops of the garnet film. The perpendicular saturation field is about 260 mT, which is very large compared to the in-plane saturation field of 5 mT. The normalized remanence (M_r/M_s) in the polar configuration (∼0.02) is about 40 times smaller than the one measured in the longitudinal configuration (∼0.85). These results reveal a strong in-plane magnetic anisotropy. The shape of the rotation (Θ_F, Θ_K) and ellipticity (E_F, E_K) of Faraday [Fig. 1(c)] and Kerr [Fig. 1(d)] spectra are in good agreement with previous studies of MO properties of Bi-YIG [25,33,34]. The comparison of the peaks positions within the Θ_F spectrum with recent experimental studies investigating the influence of the Bi content in $Bi_xY_{3-x}Fe_5O_{12}$ ($0.5 \leq x_{\mathrm{Bi}} \leq 3$) [35,36] indicates that the Bi concentration is close to $x = 1$.

Figure 2(a) shows time-resolved magneto-optical Kerr effect (TR-MOKE) measurements of the magnetization dynamics induced by 800 nm pump pulses with an energy density of $E_{\mathrm{pump}} = 9.9\ \mathrm{mJ\,cm^{-2}}$ for a magnetic field applied perpendicular to the film plane of $H_{\mathrm{ext}} = \pm 197$ mT. A detailed description of the TR-MOKE configurations with a probe pulse at 400 nm wavelength is given in the Supplemental Material [32], Note 2. During the time overlap between the pump and the probe, a large peak occurs, which can be related to the population of excited electronic states in the Fe^{3+} ion at the probe photon energy induced by two-photon absorption of the pump pulse as shown below. After this peak, complex oscillations are observed in the TR-MOKE signals. It is noteworthy that these oscillations change sign when the direction of H_{ext} is reversed, demonstrating their magnetic origin. The inset of Fig. 2(a) shows fast Fourier transform (FFT) analysis of $\Delta\Theta_K(t)$ composed of five well-separated resonance modes with different amplitudes in the frequency range between 0.7 and 13 GHz for $H_{\mathrm{ext}} = 197$ mT. The detailed characteristics of the magnetic modes can be determined by fitting the TR-MOKE signal using the sum of five time-dependent damped oscillators:

$$\Delta\Theta_K(t) = \sum_{i=0}^{4} A_i e^{-(t/\tau_i)} \sin(2\pi f_i t - \phi_i) + Be^{-Ct}, \quad (1)$$

where A_i, f_i, ϕ_i, τ_i are, respectively, the amplitude, frequency, initial phase, and decay time characterizing the precessional mode i ($i = 0$, 1, 2, 3, and 4). The term Be^{-Ct} represents a slowly changing MO background, used for better fitting but does not affect the extracted properties of the oscillations. In good agreement with the FFT analysis, the fit of the data in Fig. 2(a) yields the resonance frequencies $f_0 = 0.7$, $f_1 = 1.9$, $f_2 = 4.3$, $f_3 = 8.0$, and $f_4 = 12.8$ GHz, which we assign to the SSW modes up to 4th order. We note that the amplitudes and phases of all five magnetic resonance modes do no depend on the polarization of the pump pulses. This clearly demonstrates that the pump polarization-dependent mechanisms such as the photoinduced magnetic anisotropy [22–25] and the Cotton-Mouton effect [28,29] are not at the origin of the excitation.

The insensitivity of the excitation on the polarization of the pump suggests that the photons are absorbed and induce an ultrafast change of the magnetic anisotropy via incoherent or coherent phonons, i.e., by ultrafast heating of the lattice [18,37–39] and/or due to inverse magnetostriction induced by a hypersound wave propagating into the film [40–44]. In Bi-substituted iron garnets, the heat energy induced by a pump pulse with a wavelength of 800 nm is caused by the excitation of the phonon assisted ${}^6S \rightarrow {}^4G$ and ${}^6S \rightarrow {}^4P$ electronic $d-d$ transitions simultaneously by one- and two-photon absorption processes [45]. The phonons created during the excitation of the d-d transitions heat the lattice within hundreds of femtoseconds [45–47]. Spin precession can be triggered by ultrafast heating of the lattice via a modification of the growth induced anisotropy [48,49], which is highly sensitive to a small temperature variations in Bi-YIG [49]. The thermal energy delivered to the lattice is expected to follow the exponential attenuation of the light intensity in Bi-YIG. This leads to a nonuniform modification of the magnetic anisotropy across the Bi-YIG thickness. Such mechanism can therefore drive the generation of higher SSW modes. In order to assess the importance of coherent acoustic phonons for the excitation of SSWs [50,51], we measured the pump induced reflectivity change $\Delta R/R(t)$ [Fig. 2(b)]. Like the $\Delta\Theta/\Theta(t)$ data, the $\Delta R/R(t)$ signal shows a large peak during the overlap between the pump and probe. After the ultrafast reflectivity change $\Delta R/R(t)$ attributed to the electronic excitation following the pump pulse, oscillations of the reflectivity signal with a frequency of ~63 GHz demonstrates the propagation of a coherent phonon. The FFT spectrum of this time-domain Brillouin scattering (TDBS) signal is shown in the inset of Fig. 2(b) and fitting the reflectivity signal via

$$\Delta R(t) = Ae^{-(t/\tau)} \sin(2\pi f t - \phi) + Be^{-Ct} \quad (2)$$

yields a frequency of 63.7 GHz. The TDBS oscillations originate from an interference of the probe beam reflection at the Bi-YIG surface with the reflection from the longitudinal strain pulse propagating into the GGG. The observed Brillouin frequency perfectly matches the value $f_{\mathrm{GGG}} = 2V^L_{\mathrm{GGG}}\sqrt{n^2 - \sin^2\theta}/\lambda = 63.9$ GHz, calculated for the probe wavelength $\lambda = 400$ nm, the longitudinal sound velocity $V^L_{\mathrm{GGG}} = 6400$ m/s of GGG [52], its refractive index $n \approx 2$ [53], and the angle of incidence $\theta = 6°$. This result clearly demonstrates the generation of coherent phonons in the form of longitudinal strain pulses. Such strain pulses can modify the magnetocrystalline anisotropy and/or the stress-induced anisotropy via inverse magnetostriction and trigger a spin precession [40–43]. This excitation process can also be considered as nonuniform during the propagation of the acoustic pulse in the Bi-YIG layer and therefore contribute to the generation of the SSWs. For these reasons, we argue that the excitation of SSWs is triggered by ultrafast changes of magnetic anisotropy via laser excitation of incoherent and coherent phonons.

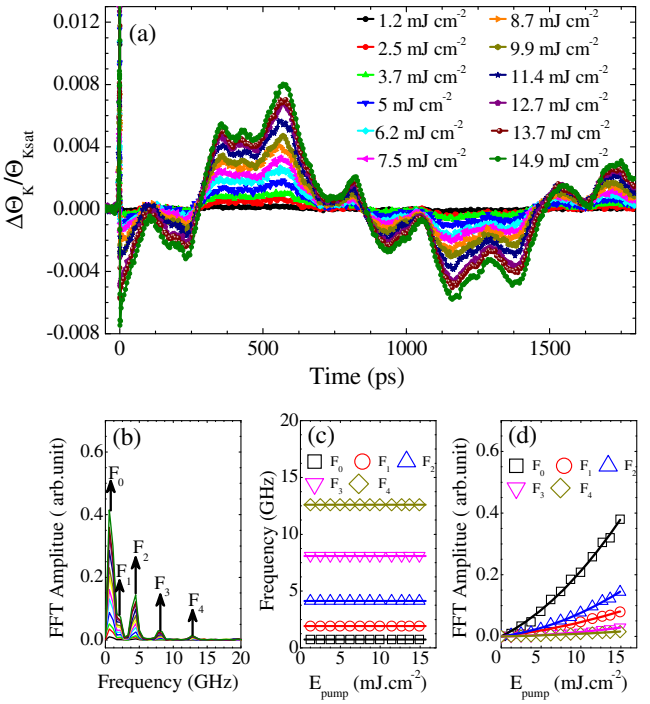

FIG. 3. Pump energy density dependence of the spin dynamics. (a) $\Delta\Theta_K/\Theta_{K\mathrm{sat}}$ measured at different E_{pump} for $H_{\mathrm{ext}} = 197$ mT. (b) FFT spectra as a function of E_{pump}. (c, d) Variation of the precession frequencies (c) and amplitudes (d) of the SSWs modes as a function of E_{pump}.

To further investigate the excitation of the magnetic resonance modes, we have measured the ultrafast magnetization dynamics as a function of E_{pump}. TR-MOKE signals measured at selected E_{pump} for $H_{\mathrm{ext}} = 197$ mT are displayed in Fig. 3(a). The results clearly show that the amplitude of the spin dynamics continuously increases with increasing E_{pump}. The detailed behavior of the oscillation frequency and amplitude as a function of E_{pump} is

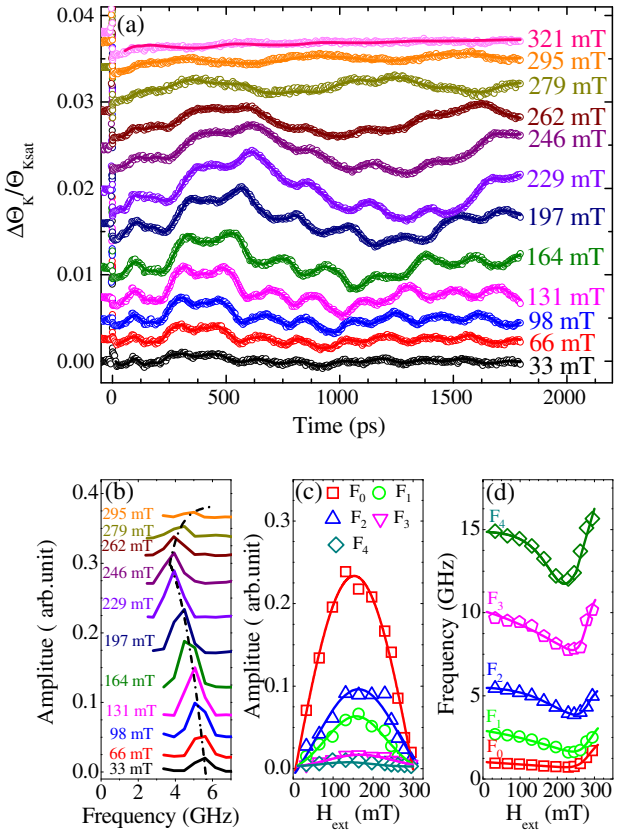

FIG. 4. Magnetic field dependence of the spin dynamics. (a) $\Delta\Theta_K/\Theta_{Ksat}$ as a function of H_{ext}. (b) Magnified view of the FFT spectra around the mode number $n = 2$. (c),(d) Field dependence of the precession amplitude (c) and frequency (d) associated to the SSWs modes. For better visualization, in (a) and (b) a vertical offset has been introduced. The dashed lines in (b) highlight the field dependence of the mode F_2. The solid lines in (c) and (d) are guide to the eye.

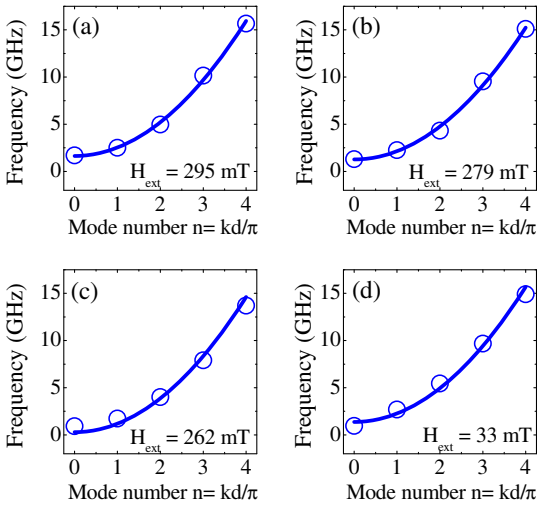

FIG. 5. Spin precession frequency as a function of the mode number measured at different values of H_{ext}. The solid lines in (a), (b) and (c) are the fits using Eq. (3). The solid line in (d) is the fit with the equation $\omega = \omega_0 + \gamma D_{ex}[(\pi/d)n]^2$.

presented in Figs. 3(c) and 3(d). The frequencies of all modes do not change with E_{pump}. On the other hand, we find that the amplitudes clearly deviate from a simple linear ($A_i = a \times E_{pump}$) or quadratic ($A_i = b \times (E_{pump})^2$) E_{pump} dependence (See Supplemental Material [32], Notes 3 and 4). However, the data can be well fitted by a second-order polynomial function ($A_i = a \times E_{pump} + b \times (E_{pump})^2$). This is in good agreement with the fact that the general process involves both a one- and two-photon absorption by the d-d transitions ${}^6S \rightarrow {}^4G$ and ${}^6S \rightarrow {}^4P$, respectively.

To confirm the SSWs nature of the observed resonance modes, we investigated the magnetic field dependence of the TR-MOKE signals. Figure 4(a) shows the results measured at selected values of H_{ext} for $E_{pump} = 9.9\ \mathrm{mJ\,cm^{-2}}$. The detailed behavior of the modes can be quantified by fitting the TR-MOKE data using Eq. (1). The field dependence of the precession amplitude [Fig. 4(c)] shows a maximum when the field approaches the out-of-plane saturation field $H_{ext} = 250$ mT. This is expected for a magnetization precession induced by an ultrafast modification of the magnetic anisotropy when H_{ext} is applied along a hard magnetization axis as in our experimental configuration [38,54]. Furthermore, the dependence of the precession frequency on the field strength [Fig. 4(d)] clearly shows that two distinct branches of the dispersion relation are excited for all the modes. In the field range below ~250 mT, the precession frequency decreases with increasing H_{ext}. We note that for the homogeneous mode ($k = 0$) in iron garnet with high in-plane magnetic anisotropy similar field dependences have been previously observed by FMR experiments [55,56]. The phenomenon was interpreted as a reorientation phase transition of the magnetic domain structure [55]. The second branch is observed for $H_{ext} > 250$ mT and it is characterized by a linearly increasing frequency with H_{ext} for all the resonance modes. This linear dispersion of the resonance modes can be well described by the Kittel formula for SSWs adapted to our experimental configuration [57,58]:

$$\omega = \gamma(H_{ext} - H_{eff} + D_{ex}k^2). \quad (3)$$

Here ω is the angular precession frequency, γ is the gyromagnetic ratio, H_{eff} is the effective field, D_{ex} is the exchange stiffness, and k represents the magnitude of the SSW's wave vector which is perpendicular to the thin film. We note that $H_{eff} = |4\pi M_s - H_u| + |H_c|$ is determined by the uniaxial (H_u) and cubic (H_c) anisotropy fields and the film thickness d fixes the wave vector $k = n\pi/d$ with n being the mode number. In order to better illustrate the SSW nature of the resonance modes, we show in Figs. 5(a)–5(c) the spin precession frequency as a function of the mode number for three different H_{ext} values above 250 mT. The experimental data exhibit a quadratic dependence on the mode number as predicted by Eq. (3). The corresponding fits obtained using Eq. (3) with $d = 135$ nm

and $(\gamma/2\pi) = 28$ GHz/T are plotted in Fig. 5. They all show an excellent agreement with the experimental results allowing us to extract $D_{ex} = (5.9 \pm 0.2)10^{-17}$ T m^2 and $H_{eff} = (0.237 \pm 0.005)$ T for all the curves. The obtained value of D_{ex} is in good agreement with the ones reported in literature for Bi-YIG [59–61], which clearly demonstrates that the observed resonance modes are indeed SSWs up to the 4th mode. We note that we have performed conventional FMR measurements based on a coplanar waveguide and a vector network analyzer on the same sample and for H_{ext} applied perpendicular to the plane of the film as in our TR-MOKE experiments. Only the SW mode corresponding to uniform magnetization precession at wave vector $k = 0$ was excited. These results demonstrate the important opportunity provided by fs laser pulses to trigger and detect SSWs in iron garnet. We also note that the difference of the angular frequency between two resonance modes n and m, i.e., $|\omega_n - \omega_m|$, at a given applied field below 250 mT is equal to $\gamma D_{ex}(\pi/d)^2|n^2 - m^2|$, which is the expected behavior for SSWs [57,58]. In other words, this means that for $H_{ext} < 250$ mT the angular frequency is given by $\omega(n) = \omega_0 + \gamma D_{ex}[(\pi/d)n]^2$. This quadratic dependence of the precession frequency as a function of the mode number is shown for $H_{ext} = 33$ mT in Fig. 5(d). This result confirms the SSW nature of the dispersion branch below 250 mT for the high-order modes ($n > 0$). We therefore prove a spin precession with a frequency of 15 GHz at very weak field [Fig. 4(d)].

In conclusion, we show that femtosecond laser pulses can trigger high frequency even and odd SSWs in a nanoscale film of Bi-YIG. Two distinct branches of the dispersion relation for all the SSW modes are distinguished by varying the strength of H_{ext}. We therefore demonstrate the possibility to trigger at very weak magnetic field of 33 mT a spin precession with a frequency of 15 GHz, which is fifteen times higher than the frequency associated with the FMR mode. We argue that the observed spin dynamics is induced by ultrafast modification of the magnetic anisotropy via incoherent and coherent phonons excited with the laser pulse. These findings reinforce the link between the fields of photonics, magnonics, and femtomagnetism, and open the door for exciting perspectives for ultrafast photo magnonic applications.

This work was supported by the ANR-NSF Project Grant No. ANR-15-CE24-0009 UMAMI, the Alexander von Humboldt Fellowship and the BMBF Project Grant No. 05K16IPA. Experiments were performed using equipment from the TUBE Dépôt et Analyse sous Ultravide de nano Matériaux funded by FEDER (EU), ANR, Région Grand Est, and Metropole Grand Nancy.

*Corresponding author.
madeb@uni-potsdam.de

[1] I. L. Markov, Nature (London) **512**, 147 (2014).
[2] V. V. Kruglyak, S. O. Demokritov, and D. Grundler, J. Phys. D **43**, 264001 (2010).
[3] B. Lenk, H. Ulrichs, F. Garbs, and M. Münzenberg, Phys. Rep. **507**, 107 (2011).
[4] A. V. Chumak, V. I. Vasyuchka, A. A. Serga, and B. Hillebrands, Nat. Phys. **11**, 453 (2015).
[5] S. Neusser and D. Grundler, Adv. Mater. **21**, 2927 (2009).
[6] A. G. Gurevich and G. A. Melkov, *Magnetization Oscillations and Waves* (CRC Press, Boca Raton, 1996).
[7] S. O. Demokritov, B. Hillebrands, and A. N. Slavin, Phys. Rep. **348**, 441 (2001).
[8] A. A. Serga, A. V. Chumak, and B. Hillebrands, J. Phys. D **43**, 264002 (2010).
[9] A. V. Chumak, A. A. Serga, and B. Hillebrands, Nat. Commun. **5**, 4700 (2014).
[10] T. Schneider, A. A. Serga, B. Leven, B. Hillebrands, R. L. Stamps, and M. P. Kostylev, Appl. Phys. Lett. **92**, 022505 (2008).
[11] C. S. Davies, A. V. Sadovnikov, S. V. Grishin, Y. P. Sharaevsky, S. A. Nikitov, and V. V. Kruglyak, IEEE Trans. Magn. **51**, 1 (2015).
[12] A. Khitun, M. Bao, and K. L. Wang, J. Phys. D **43**, 264005 (2010).
[13] I. S. Maksymov and M. Kostylev, Physica E (Amsterdam) **69**, 253 (2015).
[14] Y. Ding, T. J. Klemmer, and T. M. Crawford, J. Appl. Phys. **96**, 2969 (2004).
[15] H. Yu, O. d' Allivy Kelly, V. Cros, R. Bernard, P. Bortolotti, A. Anane, F. Brandl, F. Heimbach, and D. Grundler, Nat. Commun. **7**, 11255 (2016).
[16] J.-V. Bigot, W. Hübner, T. Rasing, and R. Chantrell, *Ultrafast Magnetism I*, Springer Proceedings in Physics (Springer International Publishing, Cham, 2015).
[17] A. Kirilyuk, A. V. Kimel, and T. Rasing, Rev. Mod. Phys. **82**, 2731 (2010).
[18] M. van Kampen, C. Jozsa, J. T. Kohlhepp, P. LeClair, L. Lagae, W. J. M. de Jonge, and B. Koopmans, Phys. Rev. Lett. **88**, 227201 (2002).
[19] B. Lenk, G. Eilers, J. Hamrle, and M. Münzenberg, Phys. Rev. B **82**, 134443 (2010).
[20] P. Němec, V. Novák, N. Tesařová, E. Rozkotová, H. Reichlová, D. Butkovičová, F. Trojánek, K. Olejník, P. Malý, R. P. Campion, B. L. Gallagher, J. Sinova, and T. Jungwirth, Nat. Commun. **4**, 1422 (2013).
[21] S. Shihab, L. Thevenard, A. Lemaître, and C. Gourdon, Phys. Rev. B **95**, 144411 (2017).
[22] F. Hansteen, A. Kimel, A. Kirilyuk, and T. Rasing, Phys. Rev. Lett. **95**, 047402 (2005).
[23] F. Hansteen, A. Kimel, A. Kirilyuk, and T. Rasing, Phys. Rev. B **73**, 014421 (2006).
[24] B. Koene, M. Deb, E. Popova, N. Keller, T. Rasing, and A. Kirilyuk, Phys. Rev. B **91**, 184415 (2015).
[25] M. Deb, M. Vomir, J.-L. Rehspringer, and J.-Y. Bigot, Appl. Phys. Lett. **107**, 252404 (2015).
[26] M. Deb, P. Molho, B. Barbara, and J.-Y. Bigot, Phys. Rev. B **94**, 054422 (2016).
[27] S. Parchenko, A. Stupakiewicz, I. Yoshimine, T. Satoh, and A. Maziewski, Appl. Phys. Lett. **103**, 172402 (2013).

[28] I. Yoshimine, T. Satoh, R. Iida, A. Stupakiewicz, A. Maziewski, and T. Shimura, J. Appl. Phys. **116**, 043907 (2014).
[29] L. Q. Shen, L. F. Zhou, J. Y. Shi, M. Tang, Z. Zheng, D. Wu, S. M. Zhou, L. Y. Chen, and H. B. Zhao, Phys. Rev. B **97**, 224430 (2018).
[30] L. Soumah, N. Beaulieu, L. Qassym, C. Carrétéro, E. Jacquet, R. Lebourgeois, J. Ben Youssef, P. Bortolotti, V. Cros, and A. Anane, Nat. Commun. **9**, 3355 (2018).
[31] P. Hansen and J. P. Krumme, Thin Solid Films **114**, 69 (1984).
[32] See Supplemental Material at http://link.aps.org/supplemental/10.1103/PhysRevLett.123.027202 for more information on the sample growth, the experimental configuration of the time resolved magneto-optical measurements, and the pump energy density dependence of the magnetization dynamics.
[33] S. Wittekoek, T. J. A. Popma, J. M. Robertson, and P. F. Bongers, Phys. Rev. B **12**, 2777 (1975).
[34] B. Koene, M. Deb, E. Popova, N. Keller, T. Rasing, and A. Kirilyuk, J. Phys. Condens. Matter **28**, 276002 (2016).
[35] C. Ming-Yau, L. Fang-Yuh, L. Da-Ren, Y. Kuang, and L. Juin-Sen, Jpn. J. Appl. Phys. **38**, 6687 (1999).
[36] M. Deb, E. Popova, A. Fouchet, and N. Keller, J. Phys. D **45**, 455001 (2012).
[37] J. Y. Bigot, M. Vomir, L. H. F. Andrade, and E. Beaurepaire, Chem. Phys. **318**, 137 (2005).
[38] A. A. Rzhevsky, B. B. Krichevtsov, D. E. Bürgler, and C. M. Schneider, Phys. Rev. B **75**, 224434 (2007).
[39] J. Kisielewski, A. Kirilyuk, A. Stupakiewicz, A. Maziewski, A. Kimel, T. Rasing, L. T. Baczewski, and A. Wawro, Phys. Rev. B **85**, 184429 (2012).
[40] A. V. Scherbakov, A. S. Salasyuk, A. V. Akimov, X. Liu, M. Bombeck, C. Brüggemann, D. R. Yakovlev, V. F. Sapega, J. K. Furdyna, and M. Bayer, Phys. Rev. Lett. **105**, 117204 (2010).
[41] J.-W. Kim, M. Vomir, and J.-Y. Bigot, Phys. Rev. Lett. **109**, 166601 (2012).
[42] J.-W. Kim, M. Vomir, and J.-Y. Bigot, Sci. Rep. **5**, 8511 (2015).
[43] M. Deb, E. Popova, M. Hehn, N. Keller, S. Mangin, and G. Malinowski, Phys. Rev. B **98**, 174407 (2018).
[44] T. L. Linnik, V. N. Kats, J. Jäger, A. S. Salasyuk, D. R. Yakovlev, A. W. Rushforth, A. V. Akimov, A. M. Kalashnikova, M. Bayer, and A. V. Scherbakov, Phys. Scr. **92**, 054006 (2017).
[45] M. Deb, P. Molho, B. Barbara, and J.-Y. Bigot, Phys. Rev. B **97**, 134419 (2018).
[46] A. V. Kimel, R. V. Pisarev, J. Hohlfeld, and T. Rasing, Phys. Rev. Lett. **89**, 287401 (2002).
[47] J. A. de Jong, A. V. Kimel, R. V. Pisarev, A. Kirilyuk, and T. Rasing, Phys. Rev. B **84**, 104421 (2011).
[48] L. A. Shelukhin, V. V. Pavlov, P. A. Usachev, P. Y. Shamray, R. V. Pisarev, and A. M. Kalashnikova, Phys. Rev. B **97**, 014422 (2018).
[49] C. S. Davies, K. H. Prabhakara, M. D. Davydova, K. A. Zvezdin, T. B. Shapaeva, S. Wang, A. K. Zvezdin, A. Kirilyuk, T. Rasing, and A. V. Kimel, Phys. Rev. Lett. **122**, 027202 (2019).
[50] Y. Hashimoto, S. Daimon, R. Iguchi, Y. Oikawa, K. Shen, K. Sato, D. Bossini, Y. Tabuchi, T. Satoh, B. Hillebrands, G. E. W. Bauer, T. H. Johansen, A. Kirilyuk, T. Rasing, and E. Saitoh, Nat. Commun. **8**, 15859 (2017).
[51] Y. Hashimoto, D. Bossini, T. H. Johansen, E. Saitoh, A. Kirilyuk, and T. Rasing, Phys. Rev. B **97**, 140404(R) (2018).
[52] V. F. Kitaeva, E. V. Zharikov, and I. L. Chistyi, Phys. Status Solidi A **92**, 475 (1985).
[53] D. L. Wood and K. Nassau, Appl. Opt. **29**, 3704 (1990).
[54] V. N. Kats, T. L. Linnik, A. S. Salasyuk, A. W. Rushforth, M. Wang, P. Wadley, A. V. Akimov, S. A. Cavill, V. Holy, A. M. Kalashnikova, and A. V. Scherbakov, Phys. Rev. B **93**, 214422 (2016).
[55] V. D. Buchel'nikov, N. K. Dan'shin, A. I. Linnik, L. T. Tsymbal, and V. G. Shavrov, J. Exp. Theor. Phys. **95**, 106 (2002).
[56] S. A. Manuilov and A. M. Grishin, J. Appl. Phys. **108**, 013902 (2010).
[57] A. H. Morrish, *The Physical Principles of Magnetism* (IEEE, New York, 2001).
[58] C. Kittel, *Introduction to Solid State Physics* (John Wiley & Sons, New York, 1986), 6th ed.
[59] S. Klingler, A. V. Chumak, T. Mewes, B. Khodadadi, C. Mewes, C. Dubs, O. Surzhenko, B. Hillebrands, and A. Conca, J. Phys. D **48**, 015001 (2015).
[60] A. Gurevich and A. Anisimov, Sov. Phys. JETP **41**, 336 (1975).
[61] G. G. Siu, C. M. Lee, and Y. Liu, Phys. Rev. B **64**, 094421 (2001).